Clim Dyn
DOI 10.1007/s00382-013-1905-7

On the ratio between shifts in the eddy-driven jet and the Hadley cell edge

Paul W. Staten · Thomas Reichler

Received: 15 October 2012 / Accepted: 1 August 2013
© Springer-Verlag Berlin Heidelberg 2013

Abstract This study explores the relationship between latitudinal shifts in the eddy-driven jet and in the Hadley cell edge as depicted in models and reanalyses. We calculate an interannual shift ratio of approximately 1.5:1 between the eddy-driven jet and the Hadley cell edge over the Southern Hemisphere during austral summer in model data. We further find that the ratio varies from season to season, with similarities between corresponding seasons over each hemisphere. Ratios are broadly consistent between models in this study, and appear to be realistic when compared to those from reanalyses. Mean tropical SSTs and the strength of zonal winds in the tropics appear to be critical to determining the ratio, while sea surface temperature variability is not. We argue that conditions in the tropics act to modulate the effect of midlatitude eddies on the Hadley cell, and the action of eddies in turn explains most of the correlated shifts from year to year. In contrast, the mean state of the tropics is a poor predictor of both the ratio of observed trends in reanalyses and the ratio of modeled externally forced shifts. We show that the ratios of modeled shifts are dependent on the type of external forcing.

P. W. Staten (✉) · T. Reichler
Department of Atmospheric Sciences, University of Utah, 135 South 1460 East Room 819, Salt Lake City, UT 84112-0110, USA
e-mail: paul.w.staten@jpl.nasa.gov

T. Reichler
e-mail: thomas.reichler@utah.edu

Present Address:
P. W. Staten
Jet Propulsion Laboratory, California Institute of Technology, 4800 Oak Grove Rd. M/S 233-304, Pasadena, CA 91109, USA

Keywords Atmospheric circulation · General circulation · Tropical-extratropical interaction · Climate change · Hadley cell · Ferrel cell

1 Introduction

Among the more robust climate projections described in the IPCC 4th assessment are poleward shifts in major circulation features and associated surface climate patterns (Solomon et al. 2007). Observations and model simulations reveal an expanding Hadley cell–which is tied to tropical surface climate–and a broadening of the dry subsidence regions along its poleward flanks (Rosenlof 2002; Hu and Fu 2007; Seidel et al. 2008; Davis and Rosenlof 2011). Rainfall over the Mediterranean, for example, is expected to decrease as local subsidence associated the Hadley cell edge encroaches on the region. The extratropical Ferrel cell is also shifting poleward (Chen and Held 2007; Lu et al. 2008, 2010; Perlwitz 2011; Staten et al. 2011b). This shift is often characterized as a trend toward a positive annular mode (AM), with falling pressure over the poles, and a corresponding poleward shift in the midlatitude jet (Kushner et al. 2001).

While it is clear that cells are shifting in latitude, what is less clear is how much, and why. For example, observational and model-based estimates of Hadley cell expansion vary by an order of magnitude (Reichler 2009; Seidel et al. 2008; Stachnik and Schumacher 2011), although Davis and Rosenlof (2011) attribute this variance to the use of varying, subjective thresholds. Calculated extratropical circulation shifts also vary between studies. Sources of this uncertainty include the shortness of the observational record, changes in the structure of midlatitude circulation (Schneider et al. 2010), and model differences.

Published online: 21 August 2013

Evaluating climate change projections, then, requires an understanding of the relevant physical climate processes, or mechanisms. While various mechanisms have been proposed to examine low or high latitude circulation shifts, no generally accepted mechanism for the shift of either the Hadley cell or the eddy driven jet yet exists. Mechanisms include that proposed by Held and Hou (1980), in which thermal wind balance, energy and angular momentum conservation determine the width of the Hadley cell. Other mechanisms include the effect of eddies to some extent (Walker and Schneider 2006; Korty and Schneider 2008; Lu et al. 2007, 2008; Held et al. 2000; Kang and Lu 2012). Hypothesized mechanisms of circulation widening in extratropics (Chen and Held 2007; Lu et al. 2010; McLandress et al. 2010; Rivire 2011) cite both linear and nonlinear wave theory. These mechanisms attempt to explain the contributions of eddy stress and nonlinear advection of angular momentum to the momentum balance in either the Hadley or Ferrel cells. It is important to note, however, that a mechanism for the dynamics of either cell is incomplete without including the effects of the other (Schneider et al. 2010).

To better understand the mechanisms behind shifts in both cells, it is useful to examine the ratio of shifts in the latitude of Hadley cell edge, and in the speed (Ceppi and Hartmann 2013) or latitude (Kang and Polvani 2010; Kidston et al. 2013) of the eddy-driven jet, or in the associated meridional circulation (as in the present study). It is hoped that understanding the mechanisms which lead to year-to-year shifts in each cell can aid in developing a theory for global circulation change. On one hand, the ratios between short-term (i.e. interannual or decadal) shifts may be unrelated to ratios of long-term shifts (i.e. climate trends). On the other hand, if the ratios between the cell shifts were similar across timescales or at least related in a straightforward manner (e.g. linearly), this would suggest that year-to-year shifts may be leveraged to explain long-term shifts.

Kang and Polvani (2010) investigate the interplay between the two cells by examining the ratio between shifts in the latitude of the eddy-driven jet and shifts in the poleward boundary of the Hadley cell. They find (1) an approximate 2:1 ratio in their respective shifts from year to year, during austral summer, and (2) inconsistent ratios of trends in the eddy-driven jet and Hadley cell. Thus, while the 2:1 ratio seems to describe year-to-year shifts well, it does not seem to describe climate trends accurately. Two possible explanations for this discrepancy may be that the circulation indices used in Kang and Polvani (2010) are sensitive to changes in circulation structure, and that the linear regression method used is sensitive to the correlation between shifts.

Kidston et al. (2013) confirm the correlation between the latitudes of the Hadley cell edge and of the surface westerlies in interannual timescales over the SH in a full GCM. Furthermore, using an idealized aquaplanet framework, they find that the correlation is dependent on the mean latitude of the Hadley cell edge and surface westerlies. Specifically, the correlation decreases—and even becomes negative—in simulations with poleward Hadley cell edges and surface westerlies.

Rather than examining the position of the midlatitude jet, Ceppi and Hartmann (2013) focus on the speed of the jet. They perform a linear regression analyses for each season, and attribute the seasonal variation of the ratio to changing wind speeds along the poleward flanks of the Hadley cell, and the resulting shifts in critical latitude for the absorption of midlatitude waves, after Chen and Held (2007). Furthermore, they note that the ratios between latitudinal shifts of the Haldey cell edge tend to be roughly proportional to changes in the midlatitude jet speed for a given season in historical CMIP5 integrations.

In the present study, we use empirical orthogonal function (EOF) analysis, rather than linear regression, to investigate the relationship between the eddy-driven jet and the Hadley cell edge. We also construct circulation indices which are less sensitive to subtle changes in jet structure than those in Kang and Lu (2012), while still examining the latitudes of the cells. Specifically, we calculate the eddy-driven jet latitude, or Ferrel cell center, using an integrated measure of the meridional overturning circulation, rather than a local wind maximum.

Aside from methodological improvements, this work expands on previous work by examining the ratio of Ferrel cell center (FC) and Hadley cell edge (HC) shifts (hereafter the FC:HC ratio) not only on interannual timescales, but also across timescales, hemispheres, and seasons. Through a regression analysis, and by applying a scaling argument by Kang and Lu (2012), we find evidence that midlatitude eddies are largely responsible for the Hadley cell edge anomalies, and interpret the FC:HC ratio to be largely a measure of the strength of the influence of extratropical eddies on the Hadley cell. In contrast to interannual ratios, ratios of trends and of equilibrium shifts due to prescribed forcings vary widely—from 1:1 to 4:1.

We explore the role of the tropics in setting the interannual FC:HC ratio, and find that the ratio depends on the mean zonal wind structure in the tropics, in agreement with Robinson (2002), Seager et al. (2003), Bordoni and Schneider (2009), Schneider and Bordoni (2008), and Kang and Lu (2012). While the modeled ratio is not critically dependent on tropical sea surface temperature variability, it is dependent on the time-mean sea surface temperature. This dependency is manifested in a strong correlation between the FC:HC ratio and the time-mean Hadley cell edge.

This paper is arranged as follows. In Sect. 2 we describe our model framework and methodology. In Sect. 3 we document the FC:HC ratios and investigate the directionality of the FC:HC relationship. In Sect. 4 we summarize our results, and discuss some of the possible connections between the HC and FC, in addition to the direct role of eddies and the modulating influence of the tropical circulation that is the focus of this paper.

2 Data and methods

We examine long control simulations from the Geophysical Fluid Dynamics Laboratory (GFDL) coupled Climate Model version 2.1 (CM2.1; see Table 1), and from its atmosphere-only component, the GFDL Atmosphere Model version 2.1 (AM2.1). In our uncoupled experiments, we prescribe seasonally varying SSTs, which repeats from year to year, as in Staten et al. (2011b).

AM2.1 has a finite volume dynamical core, with a 2° latitude by 2.5° longitude horizontal resolution, and 24 levels in the vertical (hereafter, this formulation will be referred to as L24). A modified version of AM2.1, also examined in this study, has 48 vertical levels (and is hereafter referred to as L48), with most of the additional levels being in the stratosphere (Staten et al. 2011b). For a more complete description of the model, we refer to Delworth et al. (2006) and Anderson et al. (2004).

The coupled model framework described above includes both ocean heat storage and ocean dynamics. To delineate the role of the two in setting the FC:HC ratio, we also examine output from an earlier version of the GFDL model (CM2.0-ml), coupled to a mixed layer slab ocean, using an archived simulation from the World Climate Research Programme (WCRP) Coupled Model Intercomparison Project phase 3 (CMIP3) multi-model dataset (Meehl et al. 2007). This allows us to directly examine the effect of oceanic heat storage, and to gauge the importance of ocean dynamics by comparing these results with those from the fully coupled model.

We make considerable use of a 4,000-year-long coupled pre-industrial control simulation produced using CM2.1. We also examine several uncoupled time-slice simulations created using AM2.1, each at least 500 years long, and each with prescribed concentrations of greenhouse gases (CO_2) and stratospheric ozone (O_3), and prescribed sea ice coverage and sea surface temperatures (together referred to as SSTs), all held constant from year to year (see Table 2). In an effort to keep prescribed SSTs reasonably model-consistent, we take them from multi-year average SSTs from coupled pre-industrial, twentieth century, and A1B scenario integrations performed with CM2.1. All uncoupled experiments are performed with both L24 and L48.

In order to understand the effects of external climate forcings on the general circulation, (as in Sect. 3.3), we compare pairs of time-slice simulations from Table 2 which differ in just one of the three listed forcings. For example, we attribute differences between our SST_{1870} experiment and CO_2SST_{1870} as 'due to CO_2.' We examine 24 such pairs, each with only one individual forcing differing between them. Note that the forced response in these experiments is an equilibrium response, rather than a transient response.

The GFDL models underpin much of our work. To validate our use of the GFDL model, we compare our results from the GFDL model to coupled and uncoupled simulations from models developed at the National Center for Atmospheric Research (NCAR; see to Table 1). The NCAR models we examine include one version of the

Table 1 The models used in this study

Model name	SSTs	Vertical levels	Length (years)
CM2.1	Coupled	24	4,000
AM2.1, L24	Prescribed	24	≥500 (each)
AM2.1, L48	Prescribed	48	≥500 (each)
CM2.0-ml	Mixed layer	24	50
CCSM3	Coupled	26	209
CCSM4	Coupled	26	500
CAM3	Prescribed	26	100

Table 2 AM2.1 time-slice experiments examined in this study, along with their prescribed background CO_2 concentrations, their prescribed severity of ozone depletion (O_3, expressed in proportion to the observed depletion during 1980–2000), and the year about which their prescribed SSTs are averaged

Name	CO_2 (ppm)	O_3 (×dep)	SST (year)
$0.5 \times CO_2SST_{1870}$	143	0	1870
CO_2SST_{1870}	380	0	1870
$2 \times CO_2SST_{1870}$	720	0	1870
$4 \times CO_2SST_{1870}$	1,320	0	1870
O_3SST_{1870}	286	1	1870
$CO_2O_3SST_{1870}$	380	1	1870
O_3SST_{2000}	286	1	2000
$CO_2O_3SST_{2000}$	380	1	2000
SST_{2050}	286	0	2050
$CO_{2,2050}SST_{2050}$	520	0	2050
SST_{2100}	286	0	2100
$2 \times CO_2SST_{2100}$	720	0	2100
CO_2SST_{2000}	380	0	2000
$-0.4 \times O_3SST_{1870}$	286	–0.4	1870
$2 \times O_3SST_{1870}$	286	2	1870
SST_{1870}	286	0	1870
SST_{2000}	286	0	2000
$CO_2O_3SST_{2050}$	380	1	2050

atmosphere-only model, specifically the Community Atmosphere Model version 3 (CAM3) (Hurrell et al. 2006), and two versions of the coupled model, namely the NCAR Community Climate System Model versions 3 (CCSM3) (Collins et al. 2006) and 4 (CCSM4) (Gent et al. 2011).

We further check our model results by repeating our calculations on data from the following four reanalysis datasets: the National Centers for Environmental Prediction-National Center for Atmospheric Research (NCEP/NCAR) 40 year Reanalysis Project (NNR) (Kalnay et al. 1996), the European Centre for Medium-Range Weather Forecasts (ECMWF) Interim Reanalysis (ERA Interim) (Dee and Uppala 2009), the ECMWF 40 year Reanalysis (ERA40) (Uppala et al. 2005), and the National Oceanic and Atmospheric Administration-Cooperative Institute for Research in Environmental Sciences twentieth Century Reanalysis version 2 (20CR) (Compo et al. 2011). For the sake of consistency, we only examine the years 1979–2001 in all four of the reanalyses.

2.1 Calculation of cell indices

At the core of our analysis are calculations of the latitudes of the poleward Hadley cell edges (HCs) and of the Ferrel cell centers (FCs). We calculate the HC and FC over both hemispheres (hereafter referred to as SH and NH). Since the limits and centers of these cells are calculated from threshold values (e.g. zero crossings, minima, or maxima), the calculations are sensitive to cell structure. For consistency and robustness, we average annual and decadal data for each of the four seasons (DJF, MAM, JJA, and SON) before calculating our cell indices. After we perform our threshold calculations, we remove the slowly-varying component, which is due to model drift and low-frequency climate variability. From daily indices, we remove the seasonal cycle using a gaussian filter roughly equivalent to a high-pass filter with a cutoff period of 180 days. From interannual indices, we similarly remove decadal and longer-term variability. From decadal indices, we remove century-scale and longer-term variability.

We base our analysis of cell structure on the mass meridional stream function at 500 hPa (Ψ_{500}). We calculate the HC over the SH as the positive-to-negative zero crossing south of the ITCZ, while the FC is the Ψ_{500}-weighted mean latitude of positive Ψ_{500} south of the Hadley cell. The calculations for the NH cells are the same, although the signs and directions are reversed:[1]

$$FC = \int_{-90^\circ}^{\phi_{HC}} \phi \Psi_{500} \mathrm{d}\phi \Bigg/ \int_{-90^\circ}^{\phi_{HC}} \Psi_{500} \mathrm{d}\phi \text{ for } \phi < 0, \Psi_{500} > 0,$$

or

$$FC = \int_{\phi_{HC}}^{90^\circ} \phi \Psi_{500} \mathrm{d}\phi \Bigg/ \int_{\phi_{HC}}^{90^\circ} \Psi_{500} \mathrm{d}\phi \text{ for } \phi > 0, \Psi_{500} < 0.$$

Staten et al. (2011b) made use of local minima or maxima in Ψ_{500} to estimate the latitude of the eddy-driven jet, as the two are dynamically connected, but this method proved to be sensitive to changes in the structure of the eddy-driven jet on the interannual timescales, particularly during JJA over the SH, (visible as a crescent-shaped jet-versus-HC scatter as in Fig. 2 of Kang and Polvani (2010); see Schneider et al. (2010)). The indices in this paper appear to be robust for daily, yearly, and annual averages.

2.2 Ratio estimation

Previous studies characterized the interannual relationship between the eddy-driven jet (or of the Ferrel cell center) and the HC as a ratio of the latitudinal shifts in the two. This ratio was calculated from the slope of the least squares best-fit line of the eddy-driven jet latitude versus HC scatter field (Kang and Polvani 2010; Staten et al. 2010). However, the slope of a best fit line is a monotonic function of the correlation between the dependent and independent variables. That is, as the scatter increases, the slope decreases. This also implies that the slope of the best-fit line depends on which of the two variables is considered independent. Thus, linear regression can address how the Ferrel cell varies with the Hadley cell, or vice versa, but it cannot address how both cells vary with each other. We posit that a more appropriate statistic for the co-varying fields is that which explains the most variance in the FC and the HC. Visually, this is the slope of the longest axis of a FC versus HC scatter plot. To obtain this slope, we combine the HC and FC time series into a $2 \times n$ time series, and perform an empirical orthogonal function (EOF) decomposition. This results in two two-element vectors, the first of which points in the direction of maximum variance. We call the slope of this first EOF the FC:HC ratio, or simply 'the ratio'.

The EOF method is useful mainly for describing the ratios of anomalies from year to year (hereafter termed interannual ratios), ratios of anomalies from decade to decade (decadal ratios), and ratios of anomalies from day to day (daily ratios). However, it works less well for describing the mean shifts in the Ferrel and Hadley cells brought on by external forcings. We calculate this forced

[1] We integrate to 90° in all cases, since the poleward edge of the Ferrel cell is often poorly defined. This necessitates masking out any oppositely signed polar circulation that may be present.

ratio as $(\overline{FC_2} - \overline{FC_1})/(\overline{HC_2} - \overline{HC_1})$, where overbars represent time-mean quantities, and subscripts 1 and 2 denote data taken from control and experiment datasets, respectively. Ratios of trends in the two cells (e.g. in reanalyses) are calculated as the FC trend divided by the HC trend. For all three of our ratio calculation methods, confidence intervals are calculated by bootstrapping. For each ratio estimation, we randomly subsample our data 1,000 times, without replacement, and calculate the ratio for each subsample, using the appropriate method as described above. We then take the median value as our FC:HC ratio, and 2.5th and 97.5th percentiles of the calculated ratios as our 95 % confidence interval limits.

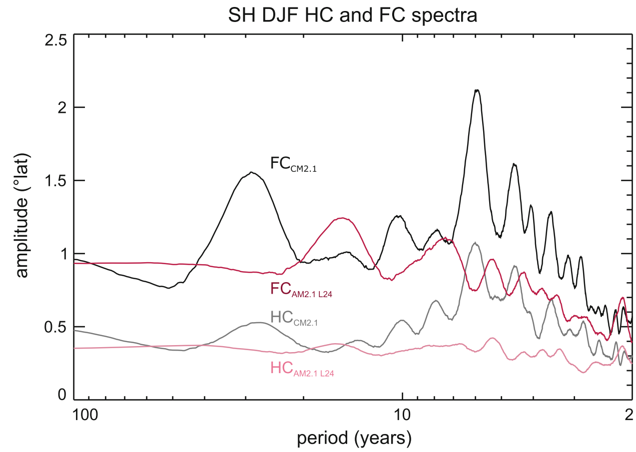

Fig. 1 Spectra of FC and HC anomalies for the coupled CM2.1 and uncoupled AM2.1 L24 control simulations for Southern Hemisphere (SH) summer (DJF)

3 Results

In this section, we first document the interannual and decadal FC:HC ratios in CM2.1 data, as described in Sect. 2. We then analyze the meaning of the ratio using regression, before discussing the ratios of trends and of forced shifts. We finally investigate the role of the tropics in setting the interannual ratio.

3.1 Documenting interannual and decadal FC:HC ratios

We start by validating our methodology, characterizing the ratios of year-to-year FC and HC anomalies for SH DJF, as has been done in previous work. These anomalies primarily exhibit red spectra up to decadal timescales in the uncoupled control simulation (see Fig. 1), and white spectra on timescales beyond. Spectra from the coupled control simulation show larger amplitudes from three to ten years, and an additional peak at about thirty years. The former timescales coincide with those of the El Niño Southern Oscillation (ENSO), while the latter peak suggests influences from decadal oceanic variability—perhaps related to the Pacific Decadal Oscillation or the Atlantic Multidecadal Oscillation. FC anomalies in both the coupled and uncoupled simulations appear generally about 1.5–2 times larger than those for the HC, depending on the timescale. Inasmuch as the two time series are correlated, the FC:HC ratios should be within this range.

Using the EOF method described in Sect. 2.2, we calculate a median interannual ratio (95 % confidence interval) of 1.48 (1.46, 1.50) during DJF for CM2.1, which is on the low end of the range of previously recorded estimates (Kang and Polvani 2010; Staten et al. 2011b) and the range just described. If we do not filter the slowly varying wind field prior to calculations, we get a ratio of about 1.7, which more closely agrees with previous studies.

The HC and FC are strongly correlated, at $r^2 = 0.75$. We also examine correlations between the HC or FC and maximum 850 hPa zonal winds and mean eddy phase speeds at 300 hPa, but r^2 values for these correlations were generally lower. For example, we calculated an r^2 value of 0.40 for the HC and maximum 850 hPa zonal winds during DJFM. During this season, then, the HC explains fractionally about twice as much of the variability in eddy-driven jet position (or FC) than in the eddy-driven jet speed.

Satisfied that our methods produce meaningful values for SH DJF, we now extend our analysis to all four seasons over both hemispheres. Figure 2 shows FC versus HC scatter plots, including the FC:HC ratio estimates for the different seasons. As explained in Sect. 2, our methods work well in most seasons; NH JJA is a striking exception. During JJA the NH Hadley cell edge is poorly defined, and a near-zero seasonal mean stream function routinely extends over 30°N–40°N. This results in a tri-modal distribution of Hadley cell edges during NH JJA (note the differing axes for the SH). Interestingly, however, inspection of Fig. 2 reveals that the middle cluster of NH JJA (centered at about 35°N, 50°N) has a slope roughly similar to that for SH DJF, hinting at a similarity in the behavior of the FC and HC during summer over both hemispheres, as with other seasons. Note also that the 1.48:1 ratio quoted above for DJF is far from universal; the ratio is generally higher for other seasons and hemispheres. Mean HC and FC positions and ratios are similar for the NCAR model data and reanalyses (not shown).

The ratios documented above are calculated from the coupled model, which produces internally generated tropical SST variability (e.g., ENSO and the Pacific decadal oscillation, or PDO). Tropical SSTs have been linked to the width of the Hadley cell (Robinson 2002; Seager et al.

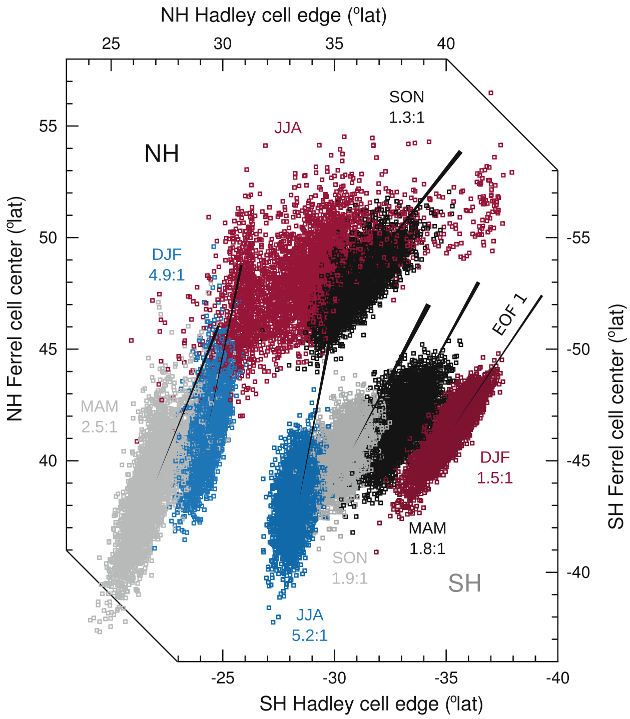

Fig. 2 Seasonal mean FC versus HC latitudes for the CM2.1 pre-industrial control for given seasons and hemispheres. The NH (SH) data are plotted on the upper-left (lower-right) axes; note that the SH axes are reversed and shifted to aid comparison. The first EOF eigenvectors for SH DJF are also shown, with the thickness increasing away from their respective origins, reflecting the estimated uncertainty in the calculated slope, or in the FC:HC ratio

2003; Lu et al. 2008), which begs the question: how does the prescribing sea surface temperatures affect the FC:HC ratio? It is conceivable that, since tropical SSTs have been linked specifically to Hadley cell width, the HC should shift less from year to year in an uncoupled simulation than in a similar coupled simulation. All else being equal, one might expect ratios to be higher in an uncoupled simulation than in a coupled simulation.

To investigate the role of SST variability, we perform our EOF analysis as above, but for uncoupled pre-industrial control simulations using both the GFDL and the NCAR models. Figure 3 shows the interannual and decadal FC:HC ratios calculated for our various datasets, along with their 95 % confidence intervals. SH DJF and SH JJA are shown. Results for NH JJA are not shown, as the HC calculation is unreliable. NH DJF results are not shown, as to a first order they are similar to those for SH JJA, but they are less certain. Examining uncoupled GFDL AM2.1 model data (AM2.1 L24 and AM2.1 L48 in Fig. 3a), we find that the uncoupled interannual FC:HC ratio during SH DJF is indeed slightly - but statistically significantly - higher than the coupled ratio, with a median estimate (95 % confidence interval) of 1.68 (1.61, 1.76) for L24, and 1.71 (1.68, 1.75) for L48.

Interannual ratios are significantly higher in AM2.1 compared to CM2.1 for all seasons over the SH. The same is true over the NH, except for JJA (in which HC calculations are problematic) and SON (for L24). But this coupled versus uncoupled relationship does not hold on decadal timescales, nor does it hold for the NCAR models. Scatter plots for uncoupled data are very similar to those in Fig. 2, with similar ratios, although with somewhat decreased scatter. While the standard deviations in HC and FC are reduced by 39 and 28 % respectively, the FC:HC ratios change little, as seen in Fig. 3.

It is important to remember that the uncoupled simulations use prescribed ten-year mean SSTs. While this ought to filter out a substantial portion of natural SST variability, it is possible that any remaining longer-term SST variability (e.g. the PDO) may alter the FC:HC ratio. This would explain not only why we see statistically significant differences in the ratio between the coupled and uncoupled simulations in some seasons, but also why these differences do not appear to be systematic between seasons and models.

In addition to investigating the role of SST variability in determining the FC:HC ratio, we examine how the ratio varies by dataset. Although our NCAR model data cover a shorter timespan (at 100–500 years) than our GFDL model data (at 2,000–4,000 years), and thus have wider confidence intervals (see Fig. 3), differences in the FC:HC ratio, at least during SH JJA, appear to be significantly model-dependent. These differences in the ratio are even larger between the model datasets and reanalyses (the gray signatures in Fig. 3). While this may indicate that the models produce a somewhat unrealistic FC:HC ratio, it may also be due to the time period examined in the reanalyses. All four reanalyses cover the same 23-year period, which may be too short a time to reliably characterize the interannual ratio. If the ratios from reanalyses can be taken at face value, however, the ratios from the NCAR models, particularly CCSM4, would appear to be more realistic than those from the GFDL models.

Finally, Fig. 3 also depicts differences in the FC:HC ratios by timescale. Interannual ratios are broadly similar to decadal ratios in models, although the difference between SH DJF ratios for CM2.1 and AM2.1 on interannual timescales decreases (and may even reverse) on decadal timescales. Examining this ratio as a function of timescale (not shown) confirms that coupled and uncoupled ratios are quite similar for timescales longer than about 7 years. The decadal ratio in reanalyses is not shown, due to the shortness of the record. Note that the decadal ratio for CAM3 over the SH during JJA is also absent from Fig. 3b, as the 95 % confidence interval for the slope varied by over 45°.

Although we also calculate daily FC:HC values, we have avoided making any serious interpretation of them,

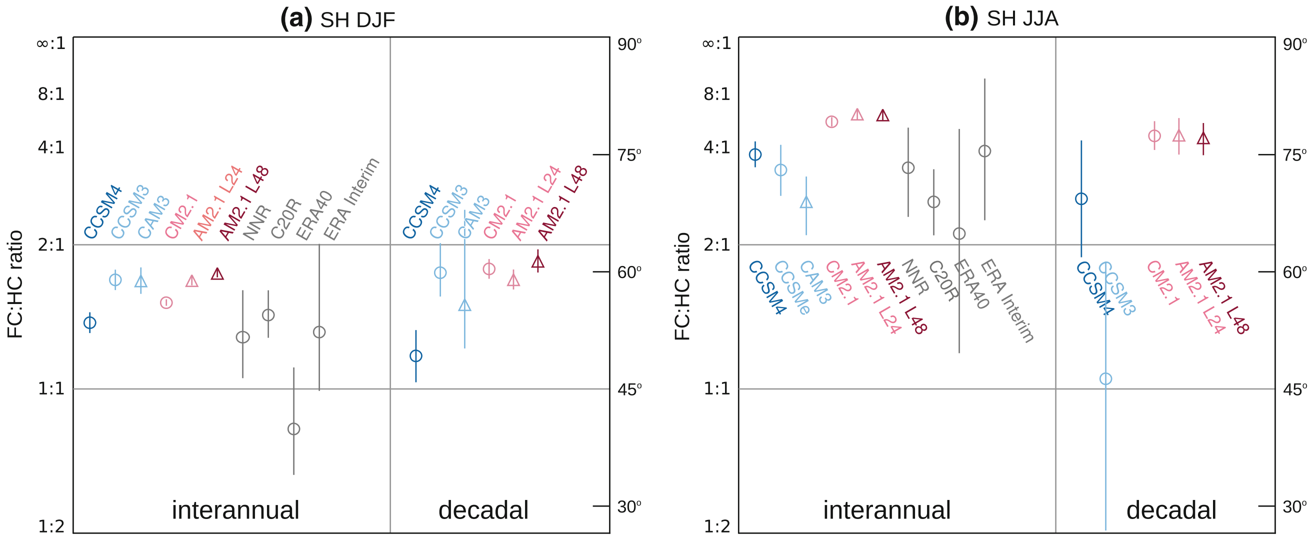

Fig. 3 FC:HC ratios and confidence intervals associated with interannual and decadal anomalies over the SH during (**a**) DJF and (**b**) JJA. The y-axis is not linear in the ratio m, but in $\tan^{-1}(m)$, and ranges from 0° to 90°. Points are only plotted if their confidence interval is reasonably narrow (less than 45°, or half the height of the plot). The *left-hand side* of each panel shows interannual ratios, while the *right-hand side* shows decadal ratios. NCAR model points are shown in *blue*, GFDL model points in *red*, and reanalyses in *gray*. Uncoupled model data are marked with *triangles*

due to the questionable meaning of the zonal mean wind field on a day-to-day basis. Over the SH, the daily ratios are lower for each season than the interannual ratios. Over the NH, we make no such generalization.

3.2 The meaning of the FC:HC ratio; a regression analysis

One advantage of employing EOF analysis is that, along with each EOF, the method produces a corresponding principal component time series. In our case, the interpretation of this time series is geometrically straightforward. The first of two EOFs calculated as described in Sect. 2 points along the direction of maximum variance, and its slope is the FC:HC ratio described previously (see the vector labeled "EOF 1" in Fig. 2). The second is orthogonal to the first, and represents a residual term, corresponding to a poleward Hadley cell edge shift, but an equatorward shift in the Ferrel cell center (or vice versa). The principal component time series associated with each EOF (named PC1 and PC2, respectively) is simply the projection of each point in FC-HC space onto the vector defined by that EOF.

We seek a physical interpretation of the FC:HC ratio by regressing sea level pressure, SSTs, and zonal mean zonal winds onto PC1, or the time series associated with the FC:HC ratio, and onto PC2, or the time series associated with the residual. Figure 4 shows the zonal mean zonal wind and eddy momentum flux convergence (EMFC) regressed onto PC1 and PC2. In the coupled case (Fig. 4a, b), shifts along the FC:HC ratio (PC1) correspond to a combination of (1) a poleward shift of the jet, a poleward shift of the associated EMFC, and decreased pressure over the pole (not shown), reminiscent of a positive annular mode, and (2) anomalous cool SSTs in the tropical Pacific (not shown) and easterlies in the tropical upper troposphere, similar to the negative phase of the El Niño-Southern Oscillation (ENSO), or to La Niña. Shifts along the residual (Fig. 4c, d) depict a contrasting sharpening and an intensification of the jet, but a similar La Niña-like wind signal in the tropics. From this, one may suppose that regressing the zonal wind field onto the FC time series alone would produce an annular mode-like pattern, while regressing onto a HC time series would produce mainly tropical easterlies. However, regressing onto either the FC or HC time series (not shown) yields a pattern very much like that in Fig. 4a, as a result of the tight correlation between the Ferrel and Hadley cells. Note that the regressions along PC1 and PC2 both yield anomalous EMFC in the tropics, and across the midlatitudes over both hemispheres. Note also the similarity of these patterns in the tropics and over the NH. This similarity suggests that tropical variability (e.g. ENSO) affects high-latitude variability over both hemispheres via interaction with midlatitude eddies.

In the uncoupled regressions, the tropical easterlies and global EMFC anomalies are absent (see Fig. 4e, f; the regression along PC2 for the uncoupled case is not shown), but the anomalies in the SH midlatitudes remain. To investigate whether ocean dynamics are required to produce the tropical signal, or whether heat storage is sufficient (see Clement et al. (2011)), we perform the same zonal wind regression analysis on 40 years of data from a mixed-layer ocean simulation (not shown). As with the uncoupled data, the tropical signal is absent. Unfortunately, this simulation is too short to clearly say whether the interannual FC:HC ratio from the mixed-layer simulation is different from either the coupled or uncoupled interannual ratios. In contrast to the mixed-layer simulation, regressing output from a simulation forced by observed SSTs once again reveals the tropical easterlies. We conclude that realistically varying SSTs, whether from observations or coupled model output, are necessary in order to capture the tropical upper-tropospheric zonal wind shifts associated with HC and FC shifts.

These figures, and the coupled versus uncoupled ratios, illustrate three important points. First, tropical SST anomalies strongly impact the strength of zonal winds within the tropics, as can be seen by comparing Fig. 4a, c. Second, zonal winds in the tropics contribute to both tropical and extratropical variability from year to year; if they did not, they would not project onto PC1. Third, in spite of the contribution from tropical winds, anomalies in the extratropical eddies alone apear to drive much of the correlated year-to-year shifts in the HC and the FC. The FC:HC ratio, then, appears to be more strongly related to extratropical—rather than tropical—variability. This can also be seen from the similarity in the coupled and uncoupeld ratios in Fig. 3.

3.3 Forced responses and observed trends

Climate change often manifests itself in trends along existing modes of variability. Climate projections, for example, include surface temperature trends resembling El

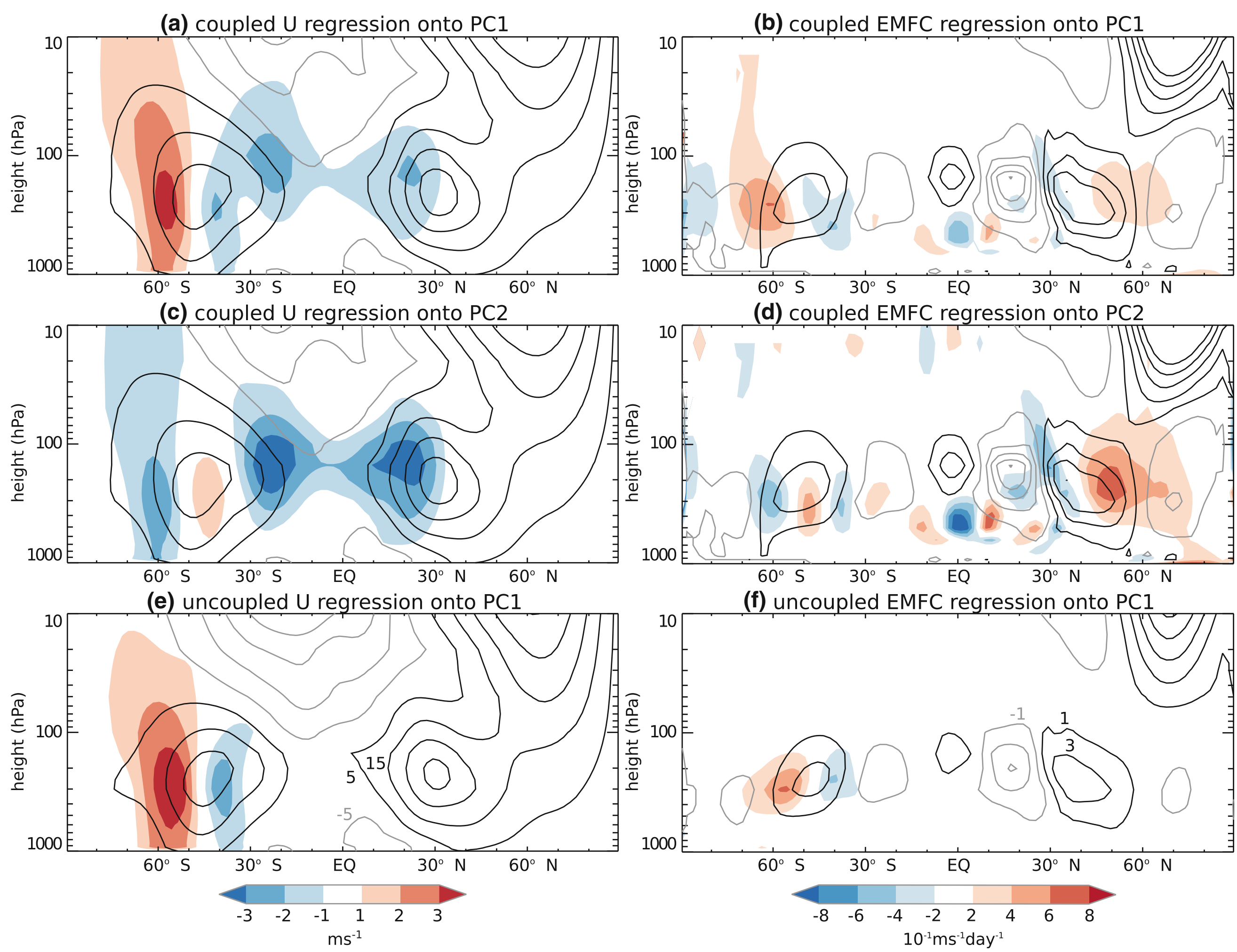

Fig. 4 Climatological DJF zonal mean (**a**, **c**, **e**) zonal winds (contours every 10 ms^{-1}) and eddy momentum flux convergence (**b**, **d**, **f**) for (**a**–**d**) coupled and (**e**, **f**) uncoupled control simulations, along with a regression (*shading*) of zonal mean zonal wind and eddy momentum flux convergence (EMFC) anomalies onto the time series of (**a**, **b**, **e**, **f**) the first EOF and (**c**, **d**) the second EOF of the SH FC versus HC time series. The regression patterns are scaled in each case to represent the wind anomalies corresponding to a 1° poleward Hadley cell edge shift

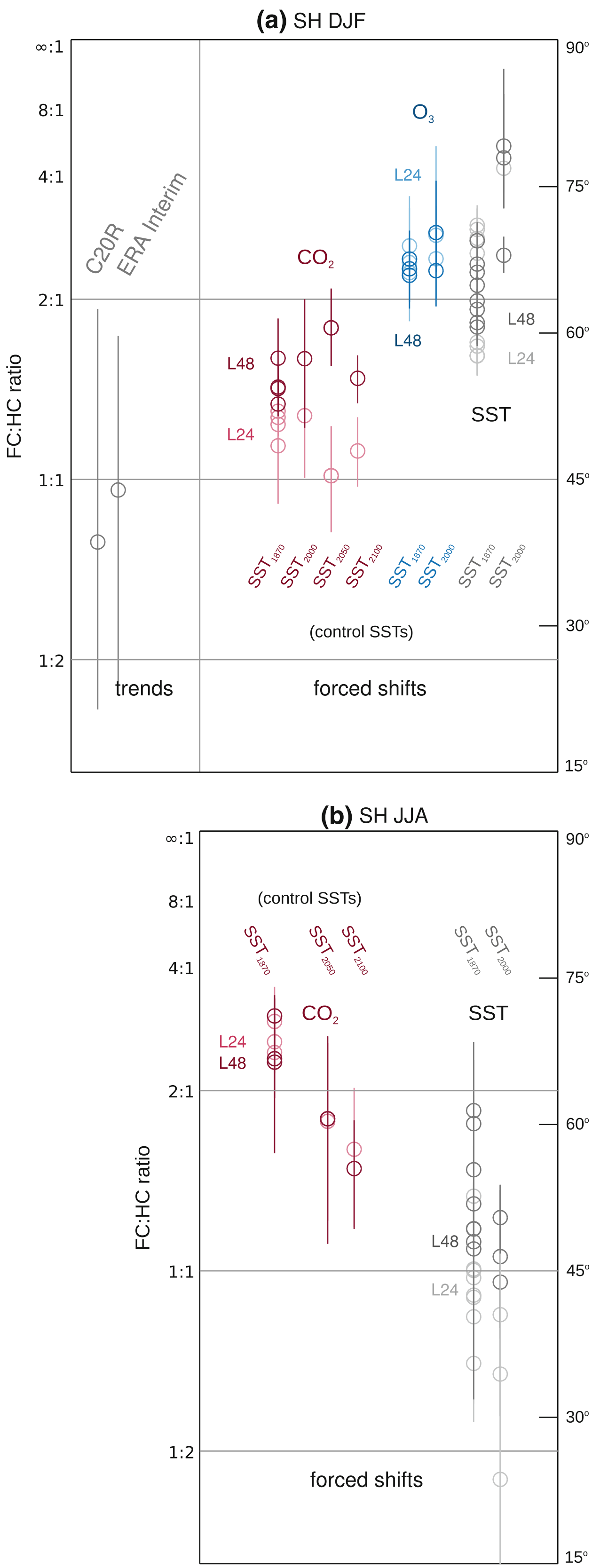

◀**Fig. 5** Ratios of observed trends and modeled forced shifts in the FC and HC, along with the confidence interval for the ratio, calculated via bootstrapping, for the SH during (**a**) DJF and (**b**) JJA. Points are only plotted if their confidence interval is reasonably narrow (less than 45°, or half the height of the plot). In the first panel, the *left-hand column* shows the ratios of trends for reanalyses (*gray*) as labeled. Ratios of trends are omitted from the second panel because the confidence intervals were wider than 45°. The *right-hand column* shows the ratios of forced shifts, calculated using the GFDL AM2.1 L24 (*light shades*) L48 (*dark shades*) models, with forcing types labeled by color. Data points are staggered horizontally according to the control SST climatology, as labeled. Points within one column may vary by the respective strength of the applied forcings, or by the background climatology aside from prescribed SSTs

Niño and sea level pressure trends resembling the arctic oscillation. Thus, there may be reason to suppose that the ratio between forced shifts in the FC and HC is similar to the interannual FC:HC ratio. Kang and Polvani (2010) investigated this, and found that the ratios of trends varied by model, although Staten et al. (2011a), using an earlier methodology, found evidence that the ratios of externally forced shifts during DJF were at least similar to the 2:1 ratio. Ceppi and Hartmann (2013) further found evidence that the mechanism from Chen and Held (2007) may play a role in determining the ratio on both interannual and climate timescales. In this section, we revisit the question of whether the ratios of the externally forced shifts in the FC and HC bear any similarity to the interannual ratios.

Figure 5 shows the ratios of trends in reanalyses, and the ratios of forced shifts in pairs of time-slice simulations that were integrated using different types of forcings (see Table 2). From this figure, we make four generalizations. First, the ratios of past trends in reanalyses are small (about 1:1) and uncertain. Second, different forcings produce different ratios. That is, some forcings have a more focused effect on either the FC or on the HC. During SH DJF, for example, ozone depletion produces noticeably higher ratios than do greenhouse gas concentration increases, indicating a particularly potent effect of ozone depletion on the midlatitude jet, relative to the Hadley cell. Third, the effects of each forcing differ by season. SST warming produces higher ratios of shifts than do CO_2 increases during SH DJF, but this relationship is reversed during SH JJA. Fourth, the ratio of shifts even for a given forcing type (e.g. for changing CO_2 concentrations) varies substantially.

Why the ratios vary so much for a given forcing is unclear, although we suspect background climatology may play a role. We find no single parameter to predict what the shift ratio for a given forcing will be. In cases, ratios appear to vary systematically between L24 and L48 formulations. The SH DJF CO_2 data in Fig. 5a show such a relationship. On the other hand, CO_2-forced ratios in the L24 and L48 simulations are quite similar during SH JJA.

We have also examined how the ratios of forced shifts relate to the magnitude of each given shift, but find little correlation. Some correlations exist between the ratios of shifts and the tropical tropospheric mean state in the control simulation, but this relationship is inconsistent between forcings and model formulations. For example, ratios of FC and HC shifts due to CO_2 for SH DJF were positively correlated with tropospheric temperature in L48, but negatively correlated in L24. This tentative relationship can be seen in Fig. 5a, as the CO_2 values are staggered, left-to-right, by the SST climatology in each respective control experiment.

Two ratios of trends are not shown in Fig. 5, but are worth mentioning. These ratios both involve SST changes from 2000 to 2050 during SH DJF, and both are negative FC:HC ratios, due to a poleward shifting HC, but an equatorward shifting FC. SST changes between 2000 and 2050 are caused by a superposition of CO_2 increases and O_3 recovery, which have competing affects on the Hadley cell and midlatitude jet (Perlwitz 2011). The resulting SSTs may likewise have an ambiguous effect on the two cells. In this case, the SST-forced cell shifts are weak, and the FC shifts slightly equatorward. Other forced experiments, including the radiatively forced trends representing greenhouse gas increases and ozone recovery from 2000 to 2050, consistently produce positive trend ratios.

Comparing the ratios of modeled forced responses to the ratios of observed trends, we find that, for SH DJF and SH JJA, CO_2-forced ratios appear to be the most similar to the ratio of trends, although these trend ratios from reanalyses have more in common with the interannual FC:HC ratios, than to the ratios of forced shifts. With just 23 years of data, the ratios of trends in reanalyses may reflect a mix of natural variability and the transient climate response. Uncertainties in the reanalysis trends are large; Hadley cell width trends over the past several decades in reanalyses are not even all of the same sign (Stachnik and Schumacher 2011).

Going back to our origional question, we find that the ratios of interannual cell shifts and the ratios of trends in cell latitude are only roughly related. While the FC tends to shift more strongly than the HC both on interannual and longer timescales, we find no systematic relationship between FC trends and HC trends, in agreement with Kang and Polvani (2010).

3.4 On the role of the tropics

Given the established connection between ENSO and the Hadley cell width, and the clear tropical signal in the regression analysis in Sect. 3.2, the similarity between the coupled and uncoupled FC:HC ratios may be surprising. In the following sections, we elaborate on the role of the tropics. We first examine the role of tropical variability, after which we examine the role of the tropical mean state.

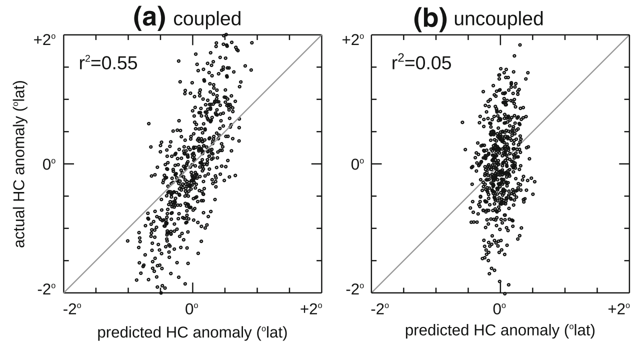

Fig. 6 Scatter plots of actual versus predicted Hadley cell anomalies over the SH during DJF in the coupled CM2.1 (*gray*) and uncoupled AM2.1 (*black*) datasets, with the explained variance shown

3.4.1 *The insensitivity of the FC:HC ratio to tropical variability*

To better understand the role tropical variability in determining the Hadley cell width from year to year, we employ a Hadley cell edge scaling from Kang and Lu (2012), which is essentially a modification of the traditional Held et al. (2000) scaling, but with an additional term to account for the mean action of eddies. Our goal here is to examine how the Hadley cell would shift from year to year, if the action of eddies on the tropics remained constant.

The traditional scaling approach is to consider, assuming angular momentum conservation, the latitude at which the overturning Hadley circulation becomes baroclinically unstable and eddy generation terminates the cell. In reality, angular momentum conservation does not hold, in large part because of the action of eddies. Kang and Lu (2012) modify the traditional equations to include the local Rossby number Ro, which describes the degree to which angular momentum conservation is valid (Walker and Schneider 2006). This yields

$$HC^2 = \frac{\phi_i^2}{2} + \frac{1}{2}\left[\phi_i^4 + \left(\frac{2gH_t}{\Omega^2 a^2 \mathrm{Ro}}\right)\right] \quad (1)$$

for the summer HC, where ϕ_i is the latitude of the ITCZ, H_t is the tropical tropopause height, g is the acceleration due to gravity, Ω is the earth's angular speed of rotation, and a is the mean radius of the earth.

To calculate the functional parameters in Eq. 1 for the SH DJF HC, we follow the procedure in Kang and Lu (2012), calculating the tropopause height after Reichler et al. (2003), averaging the height and stability terms over 20°S–40°S, and tuning *Ro* such that the predicted DJF time-mean HC matches the modeled DJF time-mean HC in each simulation. We then examine the year-to-year anomalies in the predicted and actual Hadley cells (see Fig. 6). We find the predicted and actual HCs to be fairly well correlated in the coupled simulation ($r^2 = 0.55$), confirming that the thermal structure of the tropics–specifically the latitude of the ITCZ, which explains 90 % of the variance in the predicted HC–plays a direct role in modulating the Hadley cell width. But the predicted HC varies too little, roughly by a factor of 3, as evidenced by the steep slope in Fig. 6a. The correlation disappears in the uncoupled simulation, where conditions in the deep tropics are not influenced by SST variations from year to year.

We suspect that the underwhelming performance of the Kang and Lu (2012) metric in our case is due to the timescales examined in our study. Our study analyses year-to-year changes, in which internal variability due to eddies dominates, producing an FC:HC ratio which is relatively insensitive to SST variability. Kang and Lu (2012), on the other hand, focus on 100-yr trends, in which the internal variability due to eddies is averaged out, and the direct influence of the tropics is more likely to be seen. This difference in timescales may also explain the discrepancy between the interannual ratios and ratios of trends or shifts. In the former case, internal variability in the form of extratropical eddies is manifested as the roughly 2:1 FC:HC ratio. In the latter cases, internal variability is removed by averaging, leaving systematic mean changes to contribute more strongly to the FC:HC ratio.

3.4.2 The importance of the tropical mean state

So far, our investigation of the role of the tropics in setting the FC:HC ratio has been centered on tropical variability.

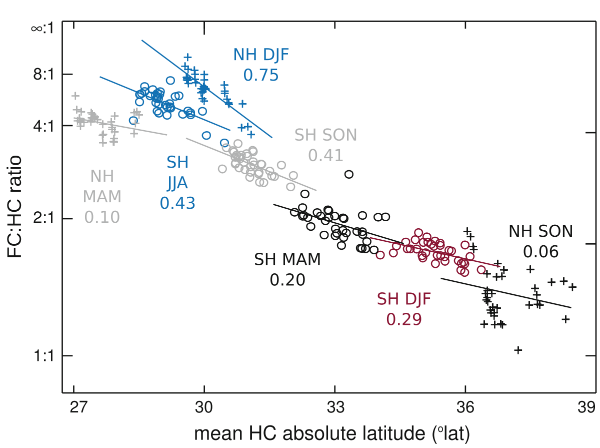

Fig. 7 The interannual FC:HC ratio versus the absolute value of the mean Hadley cell edge latitude, for the time-slice simulations shown in Table 2. NH (SH) data are marked by a + (○), and colors correspond to respective seasons as in Fig. 2. The y-axis varies as in Fig. 3, although the range is truncated, as shown. All 18 time-slice simulations are performed using L24 and L48, making 36 data points for each hemisphere and season. r^2 values for each season and hemisphere are shown under each respective label

In the following section, we more closely examine the role of the tropical mean state, similar to Kidston et al. (2013) and Ceppi and Hartmann (2013), but for each season and hemisphere.

Bordoni and Schneider (2009) and Schneider and Bordoni (2008) argue that the summertime Hadley cell extends further poleward because the stronger westerlies in the tropics allow extratropical eddies to penetrate further equatorward, removing more angular momentum, and further delaying the onset of baroclinic instability. In the context of the present study, this suggests that while mid-latitude eddies may be primarily responsible for the Hadley and Ferrel cell shifts from year to year, the mean zonal wind structure of the tropics may govern the degree to which these eddies can influence the Hadley cell.

From these studies, we conclude that seasons with a more poleward time-mean Hadley cell edge ($\overline{HC}$) are the seasons where the Hadley cell is most susceptible to mid-latitude eddies. In terms of the FC:HC ratio, seasons with a poleward $\overline{HC}$ are likely those where extratropical eddies cause year-to-year shifts in the HC which are most comparable to shifts in the FC, or when the FC:HC ratio is the lowest. More succinctly, we may expect the $\overline{HC}$ to be negatively correlated with the FC:HC ratio. These correlation values for the 18 time-slice simulations listed in Table 2, for given hemispheres and seasons, are shown in Fig. 7.

This figure neatly confirms our expectation that the $\overline{HC}$ and the FC:HC ratio are negatively correlated ($r^2 = 0.85$), even with data from both model formulations included. The relationship between the Hadley cell edge latitude and the FC:HC ratio (in degrees, or $\frac{180}{\pi}\tan^{-1}(ratio)$) appears to be roughly linear (at least in the modeled climate regimes), with the slope decreasing about 3° for every 1° latitude poleward shift of the HC. Correlations are likewise high for NCAR model data ($r^2 = 0.64$) and for reanalyses ($r^2 = 0.57$). Within seasons, correlations are moderate for the different forced experiments (with r^2 values shown in Fig. 7), confirming the importance of the tropical mean state not only for describing FC:HC ratio differences by season and hemisphere, but also for describing ratio differences by background climatology, within one season and hemisphere.

Although we focus on the relationship between the $\overline{HC}$ and the FC:HC ratio, correlations are also moderately high between the $\overline{FC}$ and the FC:HC ratio ($r^2 = 0.56$). In fact, when examining only reanalyses or NCAR model output, the correlations are slightly higher for the $\overline{FC}$ than for the $\overline{HC}$. However, within seasons, correlations are usually lower for $\overline{FC}$, compared to $\overline{HC}$ in AM2.1, and the best-fit slopes for each season do not match the slope for the seasonal cycle as well as those in Fig. 7. We note that correlations for $(\overline{FC}+\overline{HC})/2$ are similar to $\overline{HC}$, but correlations between the interannual ratio and $\overline{FC}-\overline{HC}$ or mean eddy phase speeds are substantially lower, at $r^2=0.22$ for $\overline{FC}-\overline{HC}$, and $r^2=0.04$ for phase speeds.

Our emphasis on $\overline{HC}$ contrasts with the idealized work of Kidston et al. (2013), who emphasize $\overline{FC}-\overline{HC}$. However, within a given season, r^2 values are generally smaller, and the SH DJF correlations between the FC:HC ratio and each of (1) $\overline{HC}$, (2) $\overline{FC}-\overline{HC}$, and (3) mean phase speeds cannot always be distinguished.

4 Summary and discussion

In this study, we have documented the modeled and observed ratio between shifts in the Ferrel cell center and Hadley cell edge on interannual and decadal time scales, as well as the ratio between trends in reanalyses and between externally forced shifts in time slice simulations. The interannual FC:HC ratio for SH DJF was calculated to be 1.58:1, which is in fair agreement with Kang and Polvani (2010), although our methodology yields slopes that are generally slightly lower for SH DJF. Also in agreement with their study, we find that the ratios of observed trends and of modeled externally forced shifts are highly variable, and we find no single parameter to predict the ratio of trends or of forced shifts. Our results for JJA, on the other hand, cannot be compared with theirs, as their methodology did not produce robust estimates for this season.

Kidston et al. (2013) find that the correlation between the eddy-driven jet and the HC depends on the mean position and separation of the two, using an idealized simulation. We show that, in a complex GCM, the FC:HC ratio indeed varies by season and hemisphere, and that a significant portion of the variability in the ratio within and between seasons can be accounted for by changes in the mean Hadley cell position. This suggests that mean tropical westerlies, which themselves are controlled by mean tropical SSTs, are critically important in determining the FC:HC ratio, which ratio we suggest is a manifestation of the effect of eddies on the Hadley cell, or a measure of the Hadley cell's susceptibility to the influence of midlatitude eddies. Using a metric by Kang and Lu (2012), we can explain some of the HC variability to anomalies in the tropics alone, but this metric only explains one third of the variability of the HC, and that only in the coupled simulation. We interpret this as additional evidence that changes in midlatitude eddies are primarily responsible for Hadley cell edge shifts from year to year.

Ceppi and Hartmann (2013) explicitly analyze the ability of midlatitude eddies to propagate into the Hadley cell. That is, they find that seasonal differences in the ratio between shifts in the Hadley cell edge and in lower tropospheric zonal wind maxima can be explained in part by the changing critical latitude for wave absorption on the poleward flanks of the Hadley cell, as in Chen and Held (2007). Here we find that seasonal differences in the ratio between the FC and HC are similarly sensitive to the susceptibility of the Hadley cell to dissipation by midlatitude eddies.

This work adds to an increasing body of evidence which implicates dissipation by extratropical eddies in widening the Hadley cell. The correlation between the two cells coincides with Previdi and Liepert (2007), who note that much of the variability in the extent of the Hadley cell can be explained by the state of the annular modes. The importance of zonal winds in the tropics in modulating meridional eddy propagation has been discussed by Robinson (2002), Seager et al. (2003), Walker and Schneider (2006), Lu et al. (2008), Schneider and Bordoni (2008), and Bordoni and Schneider (2009). This work compliments Kang and Lu (2012), who use a modified scaling argument to show the importance of tropical temperature structure in widening Hadley cell edge over time. We confirm that tropical temperature and wind anomalies can explain roughly a third of the Hadley cell variability, reaffirming results from Greatbatch et al. (2012), Thompson and Lorenz (2004), and Yu and Lin (2013). However, our results also suggest that on interannual timescales, the role played by dissipating extratropical eddies is dominant. Tropical-extratropical interactions are intricate indeed, and in a changing climate, the cited 2:1 ratio seems fortuitous, rather than fundamental.

Acknowledgments The authors thank two anonymous reviewers for their helpful suggestions. The work described in this publication was performed at the University of Utah department of Atmospheric Sciences. The writing and publication of this publication was supported by the JPL, Caltech, under a contract with NASA. We acknowledge the Program for Climate Model Diagnosis and Intercomparison (PCMDI) and the WCRP Working Group on Coupled Modelling (WGCM) for their roles in making available the WCRP CMIP3 multi-model dataset. We likewise acknowledge GFDL for making available their model framework and data. We thank the University of Utah Center for High Performance Computing (CHPC) for computing support. This research makes use of NCAR model data obtained from the NCAR Earth System Grid, as well as resources of the National Energy Research Scientific Computing Center, which is supported by the Office of Science of the U.S. Department of Energy under Contract No. DE-AC02-05CH11231. This research was funded in part by a NSF-GK12 grant.

References

Anderson BT, Balaji V, Broccoli AJ, Cooke WF, Delworth TL, Dixon KW, Donner LJ, Dunne KA, Freidenreich SM, Garner ST, Gudgel RG, Gordon CT, Held IM, Hemler RS, Horowitz LW, Klein SA, Knutson TR, Kushner PJ, Langenhost AR, Lau NC, Liang Z, Malyshev SL, Milly PCD, Nath MJ, Ploshay JJ, Ramaswamy V, Schwarzkopf MD, Shevliakova E, Sirutis JJ, Soden BJ, Stern WF, Thompson LA, Wilson RJ, Wittenberg AT, Wyman BL (2004) DevGGAM: the new GFDL global atmosphere and land model AM2-LM2: evaluation with prescribed SST simulations. J Clim 17(24):4641–4673. doi:10.1175/JCLI-3223.1

Bordoni S, Schneider T (2009) Regime transitions of steady and time-dependent Hadley circulations: comparison of axisymmetric and eddy-permitting simulations. J Atmos Sci 67(5):1643–1654. doi:10.1175/2009JAS3294.1

Ceppi P, Hartmann DL (2013) On the speed of the eddy-driven jet and the width of the hadley cell in the southern hemisphere. J Clim 26(10):3450–3465. doi:10.1175/JCLI-D-12-00414.1

Chen G, Held IM (2007) Phase speed spectra and the recent poleward shift of Southern Hemisphere surface westerlies. Geophys Res Lett 34(21):L21,805. doi:10.1029/2007GL031200

Clement A, DiNezio P, Deser C (2011) Rethinking the oceans role in the southern oscillation. J Clim 24(15):4056–4072. doi:10.1175/2011JCLI3973.1

Collins WD, Bitz CM, Blackmon ML, Bonan GB, Bretherton CS, Carton JA, Chang P, Doney SC, Hack JJ, Henderson TB, Kiehl JT, Large WG, McKenna DS, Santer BD, Smith RD (2006) The community climate system model version 3 (ccsm3). J Clim 19(11):2122–2143. doi:10.1175/JCLI3761.1

Compo GP, Whitaker JS, Sardeshmukh PD, Matsui N, Allan RJ, Yin X, Gleason BE, Vose RS, Rutledge G, Bessemoulin P, Brnnimann S, Brunet M, Crouthamel RI, Grant AN, Groisman PY, Jones PD, Kruk MC, Kruger AC, Marshall GJ, Maugeri M, Mok HY, Nordli O, Ross TF, Trigo RM, Wang XL, Woodruff SD, Worley SJ (2011) The twentieth century reanalysis project. Q J R Meteorol Soc 137(654):1–28. doi:10.1002/qj.776

Davis SM, Rosenlof KH (2011) A multidiagnostic intercomparison of tropical-width time series using reanalyses and satellite observations. J Clim 25(4):1061–1078. doi:10.1175/JCLI-D-11-00127.1

Dee DP, Uppala S (2009) Variational bias correction of satellite radiance data in the era-interim reanalysis. Q J R Meteorol Soc 135(644):1830–1841. doi:10.1002/qj.493

Delworth TL, Broccoli AJ, Rosati A, Stouffer RJ, Balaji V, Beesley JA, Cooke WF, Dixon KW, Dunne J, Dunne KA, Durachta JW, Findell KL, Ginoux P, Gnanadesikan A, Gordon CT, Griffies SM, Gudgel R, Harrison MJ, Held IM, Hemler RS, Horowitz LW, Klein SA, Knutson TR, Kushner PJ, Langenhorst AR, Lee HC, Lin SJ, Lu J, Malyshev SL, Milly PCD, Ramaswamy V, Russell J, Schwarzkopf MD, Shevliakova E, Sirutis JJ, Spelman MJ, Stern WF, Winton M, Wittenberg AT, Wyman B, Zeng F, Zhang R (2006) GFDL's CM2 global coupled climate models. Part I: formulation and simulation characteristics. J Clim 19(5):643–674. doi:10.1175/JCLI3629.1

Gent PR, Danabasoglu G, Donner LJ, Holland MM, Hunke EC, Jayne SR, Lawrence DM, Neale RB, Rasch PJ, Vertenstein M, Worley PH, Yang ZL, Zhang M (2011) The community climate system model version 4. J Clim 24(19):4973–4991. doi:10.1175/2011JCLI4083.1

Greatbatch RJ, Gollan G, Jung T, Kunz T (2012) Factors influencing northern hemisphere winter mean atmospheric circulation anomalies during the period 1960/61 to 2001/02. Q J R Meteorol Soc 138(669):1970–1982. doi:10.1002/qj.1947

Held IM, Hou AY (1980) Nonlinear axially symmetric circulations in a nearly inviscid atmosphere. J. Atmos. Sci. 37(3):515–533. doi:10.1175/1520-0469(1980)037<0515:NASCIA>2.0.CO;2

Held IM, Salmon R, Fields J, Thiffeault JL (2000) The general circulation of the atmosphere. In: The general circulation of the atmosphere: 2000 program in geophysical fluid dynamics, Tech. Rep. WHOI-2001-03, pp. 1–54. Woods Hole Oceanogr. Inst., Woods Hole, Mass. http://hdl.handle.net/1912/15

Hu Y, Fu Q (2007) Observed poleward expansion of the hadley circulation since 1979. Atmos Chem Phys 7(19):5229–5236. http://www.atmos-chem-phys.net/7/5229/2007/

Hurrell JW, Hack JJ, Phillips AS, Caron J, Yin J (2006) The dynamical simulation of the community atmosphere model version 3 (cam3). J Clim 19(11):2162–2183. doi:10.1175/JCLI3762.1

Kalnay E, Kanamitsu M, Kistler R, Collins W, Deaven D, Gandin L, Iredell M, Saha S, White G, Woollen J, Zhu Y, Leetmaa A, Reynolds R, Chelliah M, Ebisuzaki W, Higgins W, Janowiak J, Mo KC, Ropelewski C, Wang J, Jenne R, Joseph, D.: The NCEP/NCAR 40-year Reanalysis Project. Bull Amer Meteor Soc 77(3):437–471 (1996). doi:10.1175/1520-0477(1996)077<0437:TNYRP>2.0.CO;2

Kang SM, Lu J (2012) Expansion of the hadley cell under global warming: winter versus summer. J Clim 25(24):8387–8393. doi:10.1175/JCLI-D-12-00323.1

Kang SM, Polvani LM (2010) The interannual relationship between the latitude of the eddy-driven jet and the edge of the Hadley cell. J Clim 24(2):563–568. doi:10.1175/2010JCLI4077.1

Kidston J, Cairns CW, Paga P (2013) Variability in the width of the tropics and the annular modes. Geophys Res Lett. doi:10.1029/2012GL054165

Korty RL, Schneider T (2008) Extent of Hadley circulations in dry atmospheres. Geophys Res Lett. 35(23):L23803. doi:10.1029/2008GL035847

Kushner PJ, Held IM, Delworth TL (2001) Southern Hemisphere atmospheric circulation response to global warming. J Clim 14(10):2238–2249. doi:10.1175/1520-0442(2001)014<0001:SHACRT>2.0.CO;2

Lu J, Chen G, Frierson DMW (2008) Response of the zonal mean atmospheric circulation to El Niño versus global warming. J Clim 21(22):5835–5851. doi:10.1175/2008JCLI2200.1

Lu J, Chen G, Frierson DMW (2010) The position of the midlatitude storm track and eddy-driven westerlies in aquaplanet AGCMs. J Atmos Sci 67(12):3984–4000. doi:10.1175/2010JAS3477.1

Lu J, Vecchi GA, Reichler T (2007) Expansion of the Hadley cell under global warming. Geophys Res Lett 34(6):L06,805. doi:10.1029/2006GL028443

McLandress C, Shepherd TG, Scinocca JF, Plummer DA, Sigmond M, Jonsson AI, Reader MC (2010) Separating the dynamical effects of climate change and ozone depletion. Part II: Southern Hemisphere troposphere. J Clim 24(6):1850–1868. doi:10.1175/2010JCLI3958.1

Meehl GA, Covey C, Taylor KE, Delworth T, Stouffer RJ, Latif M, McAvaney B, Mitchell JFB (2007) The WCRP CMIP3 multi-model dataset: a new era in climate change research. Bull. Amer. Meteor. Soc. 88(9):1383–1394. doi:10.1175/BAMS-88-9-1383

Perlwitz J (2011) Atmospheric science: Tug of war on the jet stream. Nat Clim Chang 1(1):29–31. doi:10.1038/nclimate1065

Previdi M, Liepert BG (2007) Annular modes and Hadley cell expansion under global warming. Geophys Res Lett 34(22):L22,701. doi:10.1029/2007GL031243

Reichler T (2009) Chapter 7—changes in the atmospheric circulation as indicator of climate change. In: Letcher TM (ed) Climate change. Elsevier, Amsterdam, pp. 145–164. doi:10.1016/B978-0-444-53301-2.00007-5

Reichler T, Dameris M, Sausen R (2003) Determining the tropopause height from gridded data. Geophys Res Lett 30(20):2042. doi:10.1029/2003GL018240

Rivire G (2011) A dynamical interpretation of the poleward shift of the jet streams in global warming scenarios. J Atmos Sci 68(6):1253–1272. doi:10.1175/2011JAS3641.1

Robinson WA (2002) On the midlatitude thermal response to tropical warmth. Geophys Res Lett 29(8):1190. doi:10.1029/2001GL014158

Rosenlof KH (2002) Transport changes inferred from HALOE water and methane measurements. J Meteor Soc Japan 80(4B): 831–848. doi:10.2151/jmsj.80.831

Schneider T, Bordoni S (2008) Eddy-mediated regime transitions in the seasonal cycle of a Hadley circulation and implications for monsoon dynamics. J Atmos Sci 65(3):915–934. doi:10.1175/2007JAS2415.1

Schneider T, O'Gorman PA, Levine XJ (2010) Water vapor and the dynamics of climate changes. Rev Geophys 48(3):RG3001. doi:10.1029/2009RG000302

Seager R, Harnik N, Kushnir Y, Robinson W, Miller J (2003) Mechanisms of hemispherically symmetric climate variability. J Clim 16(18):2960–2978. doi:10.1175/1520-0442(2003)016<2960:MOHSCV>2.0.CO;2

Seidel DJ, Fu Q, Randel WJ, Reichler TJ (2008) Widening of the tropical belt in a changing climate. Nat Geosci 1(1):21–24. doi:10.1038/ngeo.2007.38

Solomon S, Qin D, Manning M, Chen Z, Marquis M, Averyt KB, Tignor M, Miller HL (2007) The physical science basis. Contribution of working group I to the fourth assessment report of the intergovernmental panel on climate change. In: IPCC 2007: climate change 2007. Cambridge University Press, Cambridge, United Kingdom and New York, NY, USA. http://www.ipcc.ch/publications_and_data/ar4/wg1/en/contents.html

Stachnik JP, Schumacher C (2011) A comparison of the Hadley circulation in modern reanalyses. J Geophys Res 116:D22102. doi:10.1029/2011JD016677

Staten PW, Reichler T, Lu J (2010) Understanding the direct and indirect circulation response to radiative forcings. In: AGU fall meeting. http://www.inscc.utah.edu/pstaten/talks/Staten_2010_AGU_A33A-0149.pdf

Staten PW, Reichler T, Lu J (2011) Southern hemisphere circulation shifts in a warming climate. In: World climate research program open science conference. http://www.inscc.utah.edu/pstaten/talks/C36_Staten_Th54A.pdf

Staten PW, Rutz JJ, Reichler T, Lu J (2011) Breaking down the tropospheric circulation response by forcing. Clim Dyn 39:2361–2375. doi:10.1007/s00382-011-1267-y

Thompson DWJ, Lorenz DJ (2004) The signature of the annular modes in the tropical troposphere. J Clim 17(22):4330–4342. doi:10.1175/3193.1

Uppala SM, KÅllberg PW, Simmons AJ, Andrae U, Bechtold VDC, Fiorino M, Gibson JK, Haseler J, Hernandez A, Kelly GA, Li X, Onogi K, Saarinen S, Sokka N, Allan RP, Andersson E, Arpe K, Balmaseda MA, Beljaars ACM, Berg LVD, Bidlot J, Bormann N, Caires S, Chevallier F, Dethof A, Dragosavac M, Fisher M, Fuentes M, Hagemann S, Hlm E, Hoskins BJ, Isaksen L, Janssen PAEM, Jenne R, Mcnally AP, Mahfouf JF, Morcrette JJ, Rayner NA, Saunders RW, Simon P, Sterl A, Trenberth KE, Untch A, Vasiljevic D, Viterbo P, Woollen J (2005) The ERA-40 re-analysis. Q J R Meteorol Soc 131(612):2961–3012. doi:10.1256/qj.04.176

Walker CC, Schneider T (2006) Eddy influences on Hadley circulations: simulations with an idealized GCM. J Atmos Sci 63(12):3333–3350. doi:10.1175/JAS3821.1

Yu B, Lin H (2013) Tropical american-atlantic forcing of austral summertime variability in the southern annular mode. Geophys Res Lett pp. n/a–n/a. doi:10.1002/grl.50231